

See discussions, stats, and author profiles for this publication at: <https://www.researchgate.net/publication/259334914>

Selective Optical Sensing of Hg(II) in Aqueous Media by H-Acid/SBA-15: A Combined Experimental and Theoretical Study

ARTICLE in THE JOURNAL OF PHYSICAL CHEMISTRY C · APRIL 2013

Impact Factor: 4.77 · DOI: 10.1021/jp401479z

CITATIONS

15

READS

117

4 AUTHORS:



Pezhman Zarabadi-Poor

13 PUBLICATIONS 132 CITATIONS

[SEE PROFILE](#)



Alireza Badiei

University of Tehran

238 PUBLICATIONS 1,680 CITATIONS

[SEE PROFILE](#)



Ali Akbar Yousefi

Iran Polymer and Petrochemical Institute

87 PUBLICATIONS 1,039 CITATIONS

[SEE PROFILE](#)



Joaquin Barroso-Flores

Universidad Nacional Autónoma de México

19 PUBLICATIONS 78 CITATIONS

[SEE PROFILE](#)

Selective Optical Sensing of Hg(II) in Aqueous Media by H-Acid/SBA-15: A Combined Experimental and Theoretical Study

Pezhman Zarabadi-Poor,[†] Alireza Badei,^{*,†} Ali Akbar Yousefi,[‡] and Joaquín Barroso-Flores,[§]

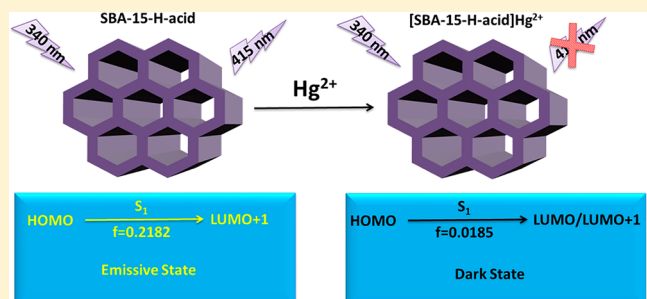
[†]School of Chemistry, College of Science, University of Tehran, Tehran, Iran

[‡]Department of Plastic Materials Processing and Engineering, Iran Polymer and Petrochemical Institute, Tehran, Iran

[§]Centro Conjunto de Investigación en Química Sustentable UAEM-UNAM, Car. Toluca-Atlacomulco, Km 14.5 Unidad San Cayetano, Personal de la UNAM, Toluca 50200, Estado de México, México

Supporting Information

ABSTRACT: The H-acid dye intermediate was successfully attached to the SBA-15 mesoporous silica surface in a two-step modification process. Synthesized materials were characterized using several techniques including Fourier transform infrared spectroscopy, N₂ adsorption–desorption measurements, small-angle X-ray scattering, transmission electron microscopy, and thermogravimetric analysis. The fluorescent sensing properties were examined in the final product toward several metal ions and showed high selectivity for Hg²⁺. Computational studies were performed in order to obtain a detailed electronic description of the quenching mechanism of H-acid fluorescence by Hg²⁺ as well as studying the structure and bonding in the [H-acid]Hg²⁺ complex.



1. INTRODUCTION

The SBA-15^{1,2} mesoporous silica has proven to be an excellent support for lots of applications due to its high surface area, uniform open pores, thick walls, high hydrothermal and thermal stability, optical transparency in visible region, and biocompatibility.³ In order to make these kinds of materials usable in applications such as catalysis,^{4–6} solid phase microextraction,⁷ optical sensors,⁸ etc., the surface modification procedure is vastly employed to introduce different functional groups into the mesoporous silicas via grafting or co-condensation approaches.⁹ Fluorescence spectroscopy is one of the most popular techniques in sensing applications; functionalization of SBA-15 and other mesoporous silicas by organic fluorophores has attracted a great deal of attention because it provides selective, sensitive, low cost, and rapid response optical sensors.^{10–12} Because of the toxicity of heavy metal ions for living organisms and the human body, synthesis of new fluorescent sensors for optical detection of metal ions such as Cu²⁺, Zn²⁺, and Hg²⁺, among others, has become a broad field of research.^{10,13–18} Among the heavy metal ions, mercury in its different forms such as metallic, inorganic, and organometallic is very hazardous and can cause serious problems,¹⁹ i.e., acrodynia (pink disease), Hunter–Russell syndrome, and Minamata disease. Therefore, detection and elimination of mercury compounds is still an interesting and undergoing research field.

Up to now, several SBA-15-based optical sensors have been reported for the fluorimetric detection of Hg²⁺ ions. These optical sensors consist of a fluorescent molecule, i.e., pyrene,⁸ rhodamine,^{20,21} naphthalimide,²² and others, attached to the SBA-15. Although reported sensors exhibited satisfying results on selective and sensitive detection of Hg²⁺ ions in water, production cost of

sensors and availability of the sensing probe remain a challenge; further research in design and synthesis of new sensors is required. Young reported the selective detection of Hg²⁺ in aqueous solution using a dye intermediate, H-acid, and obtained satisfying results.²³ Then, Sun et al. incorporated the H-acid into a layered double hydroxide and examined the applicability of synthesized composite for Hg²⁺ selective detection on a thin film.²⁴

Herein, we report the synthesis of H-acid modified SBA-15 (SBA-15-HA) to enable the usage of this optical Hg²⁺ sensor in a wider practical field. The synthesized materials were fully characterized and the recognition ability of SBA-15-HA as a chemosensor was investigated using fluorescence spectroscopy. According to our knowledge, the mechanism of mercury sensing by H-acid as well as their bonding nature remains an open question. Therefore, quantum-mechanical calculations were performed in order to provide more detailed information on the aforementioned issues.

2. EXPERIMENTAL AND COMPUTATIONAL PROCEDURES

2.1. Materials. Tetraethyl orthosilicate (TEOS, Merck) was employed as a silica source; poly(ethylene glycol)-block-poly(propylene glycol)-block-poly(ethylene glycol) (P123, Aldrich) was used as a structure-directing agent; and 3-(chloropropyl)-trimethoxysilane (CPTMS, Merck), 1-amino-8-naphthol-3,6-disulfonic acid monosodium salt (H-acid or ANDS, Merck),

Received: February 10, 2013

Revised: April 8, 2013

Published: April 15, 2013



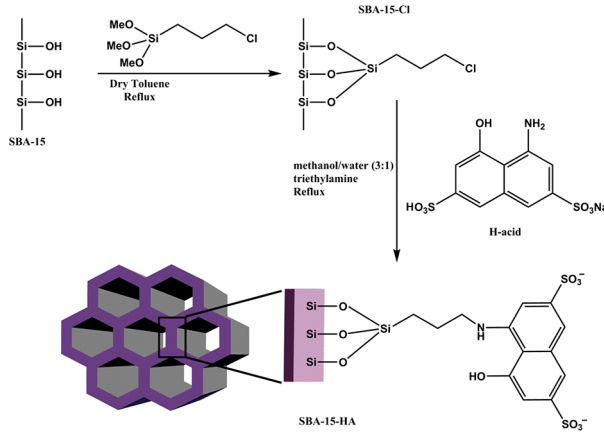
concentrated hydrochloric acid (Merck), and ethanol (Merck) were used as received from suppliers. All other materials including metals salts were of analytical grade and used as purchased from Merck and Sigma-Aldrich without further purification.

2.2. Synthesis of SBA-15. The SBA-15 was synthesized based on our previous reports.^{7,25} In a typical synthesis, Pluronic P123 (2 g) was dissolved in deionized water (2 mL) and HCl (30 g, 2 mol L⁻¹) was added consequently. Then, TEOS (4 g) was added dropwise while the reaction mixture was kept stirred at 35 °C. After adding the TEOS, the resultant mixture was stirred at 35 °C for 24 h. In the next step, the resultant mixture was transferred to a Teflon-lined autoclave. The reactor was sealed and maintained at 100 °C for 48 h. The white solid was filtered off after allowing the reactor to cool down to room temperature. The product was then washed several times with deionized water. The template was removed using a Soxhlet extractor and ethanol as solvent. Finally, the product was calcined at 600 °C for 6 h.

2.3. Synthesis of SBA-15-Cl. The synthesis procedure for the modification of the SBA-15 with the chloropropyl moiety is as follows: the synthesized SBA-15 (1 g) and dry toluene (100 mL) were placed in a two-neck round-bottom flask. The mixture was stirred under heating at 40 °C to achieve a homogeneous dispersion. Afterward, CPTMS (1 mL, about 5 mmol) was added, and then the reaction mixture refluxed for 24 h. Then, the solid was filtered and washed several times with fresh dry toluene in order to remove unreacted CPTMS. Finally, the product was dried at 100 °C overnight.

2.4. Synthesis of SBA-15-HA. The H-acid-modified SBA-15 (SBA-15-HA) was synthesized according to the following procedure. The H-acid (10 mmol) was dissolved in methanol and water (3:1, v/v). Then, SBA-15-Cl (5 g) was added to the above solution and was stirred to obtain a well-dispersed mixture; after that, triethylamine (10 mmol) was added, and the reaction mixture was stirred under reflux conditions for 24 h. The solid was filtered and washed several times with deionized water and methanol to remove unreacted H-acid. The resultant violet solid was dried at 100 °C overnight and was kept for further analyses and applications. The schematic representation of SBA-15-HA synthesis procedure is depicted in Scheme 1.

Scheme 1. Schematic Representation of SBA-15-HA Synthesis Procedure



2.5. Characterization Techniques. Small-angle X-ray scattering (SAXS) measurements were performed on a Hecus S3-MICROpix SAXS diffractometer using Cu K α radiation ($\lambda = 1.542 \text{ \AA}$). The N₂ adsorption-desorption isotherms were

obtained using a BELSORP-miniII instrument at liquid nitrogen temperature (-196°C). All samples were degassed at 100 °C before performing measurements. The Brunauer–Emmet–Teller (BET) and Barrett–Joyner–Halenda (BJH) equations were applied on sorption data using BELSORP analysis software to calculate physical properties of materials such as specific surface area, pore diameter, pore volume, and pore size distribution. The Fourier transform infrared (FT-IR) spectra of samples were recorded on an EQINOX50 Bruker apparatus. Transmission electron microscopy (TEM) was performed on a Technai G5 instrument at an accelerating voltage of 300 kV. Samples were dispersed in ethanol using an ultrasonic bath, and a drop of the ethanol mixture was placed on a lacey carbon-coated copper grid for analysis. Thermogravimetric analysis (TGA) was carried out in a PerkinElmer Pyris Diamond instrument from ambient temperature to 800 °C with a ramp rate of 10 °C/min. Fluorescence spectra were recorded on a PerkinElmer LB50 instrument.

2.6. Computational Details. In order to have better insight on the electronic properties of H-acid and its complex with Hg²⁺ ions, quantum mechanical calculations were carried out with the density functional theory (DFT) and time-dependent density functional theory (TD-DFT) in water using Gaussian 09 computational package.²⁶ We have chosen parameter-free PBE0 hybrid functional²⁷ for all DFT and TD-DFT calculations combined with Pople's split-valence double- ζ 6-31++G** basis set^{28,29} for all atoms except mercury. The Dunning's double- ζ augmented correlation consistent polarized basis set (aug-cc-pVDZ) along with the corresponding effective core potentials (ECP) were used for Hg.^{30,31} All geometries were optimized in gas phase and then further optimized in water using default polarized continuum model (PCM)³² implemented in Gaussian 09 program. Subsequent vibrational frequencies were calculated at the same level of theory in order to verify that the stationary points found are local minima on the potential energy surface. The vertical excitation energies were calculated using the TD-DFT method. The Mayer bond orders were calculated using MultiWFN.³³

3. RESULTS AND DISCUSSION

3.1. SAXS and N₂ Adsorption–Desorption Measurements. The small-angle X-ray scattering (SAXS) patterns of SBA-15, SBA-15-Cl, and SBA-15-HA are given in Figure 1 in

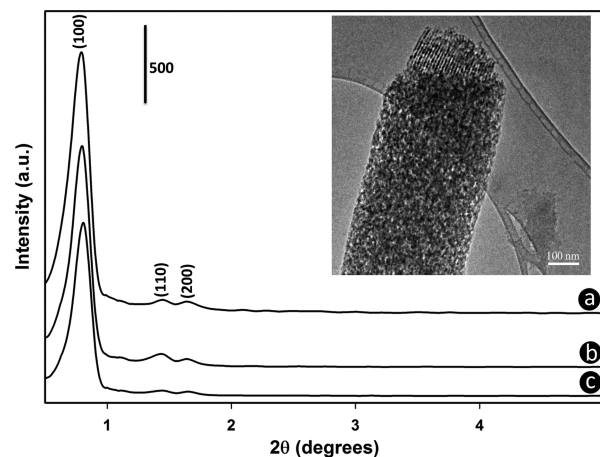


Figure 1. SAXS patterns of (a) SBA-15, (b) SBA-15-Cl, and (c) SBA-15-HA (inset: TEM image of SBA-15).

which the effect of surface modifications on the structure of materials is observed. All synthesized materials exhibit three

well-resolved characteristic diffractions peaks that can be indexed as (100), (110), and (200) diffractions that can be referred to typical two-dimensional hexagonal lattice of SBA-15 materials with $P6mm$ space group² which is in consistence with the TEM image (Figure 1 inset) exhibiting highly ordered channels of SBA-15. Indeed, two important points are observed by comparing the SAXS patterns of SBA-15, SBA-15-Cl, and SBA-15-HA; the aforementioned peaks are present in all patterns, and the intensity of peaks decreases after each step of modification.

The former one shows that the long-range hexagonal symmetry of SBA-15 was preserved after chemical modifications. The latter observation indicates that mesoporous framework has not been destroyed, but the crystallinity decreased. It is attributed to larger X-ray scattering contrast between SBA-15 walls and open pores than that exists between the SBA-15 walls and the organic functional groups. These observations reveal that the grafting was successfully done and took place inside the mesoporous channels.

The changes in porosity and surface physical properties of the synthesized materials were further investigated by nitrogen adsorption–desorption technique. The adsorption–desorption isotherms of materials are provided in Figure 2. The SBA-15

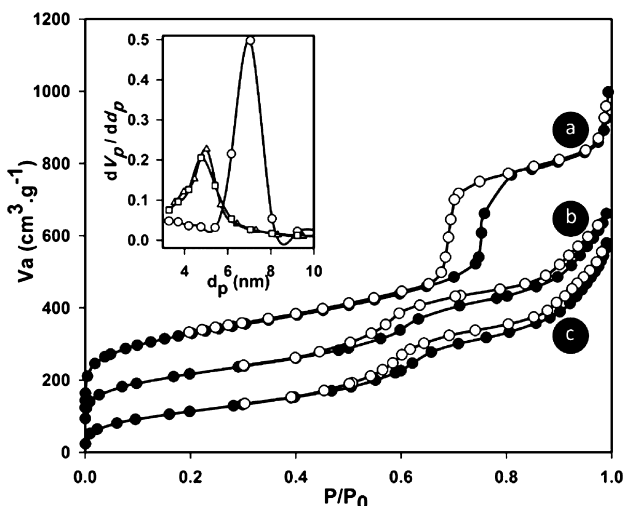


Figure 2. N_2 adsorption–desorption isotherms of (a) SBA-15, (b) SBA-15-Cl, and (c) SBA-15-HA (inset: the BJH pore size distribution of SBA-15 (\circ), SBA-15-Cl (\triangle), and SBA-15-HA (\square))).

material shows a typical type IV standard IUPAC isotherm which corresponds to mesoporous materials. The observed H1 hysteresis loop at high relative pressures indicates capillary condensation occurring within uniform pores.³⁴

The SBA-15-Cl and SBA-15-HA materials also represent similar isotherms with lower level of gas adsorption as well as hysteresis loops with lower height. Since the hysteresis loops are still present in functionalized materials, it can be concluded that the pore blocking did not happen during the modification process and therefore the pores are still open and accessible for further applications of produced materials. These observations indicate the successful attachment of functional organic materials to the SBA-15 material which caused the shrinkage of the pore volume as well as decrease the specific surface area of the modified materials.

The structural parameters including d_{100} , specific surface area, pore volume, pore diameter, lattice parameter, and wall thickness obtained from SAXS and sorption measurements are given in Table 1. Generally, the peak position of (100) reflection indicates

Table 1. Structural Parameters of SBA-15, SBA-15-Cl, and SBA-15-HA

sample	S_{BET}^a ($\text{m}^2 \text{g}^{-1}$)	d_p^b (nm)	V_p^c ($\text{cm}^3 \text{g}^{-1}$)	d_{100}^d (nm)	a_0^e (nm)	d_w^f (nm)
SBA-15	783	7.05	1.29	10.98	12.68	5.63
SBA-15-Cl	528	5.03	0.91	10.87	12.55	7.52
SBA-15-HA	419	4.76	0.89	10.74	12.40	7.64

^aBET specific surface area obtained from adsorption isotherm data within the P/P_0 range of 0.05–0.35. ^bBJH pore diameter obtained from desorption isotherm. ^cPore volume obtained from BJH analysis on desorption isotherm. ^d d (100) spacing obtained from $n\lambda = 2d \sin \theta$ equation. ^eUnit-cell parameter obtained using $a_0 = 2d_{100}/\sqrt{3}$ equation. ^fWall thickness obtained from $d_w = a_0 - d_p$ equation.

the d_{100} spacing for synthesized materials using Bragg's equation. The pure SBA-15 material shows a d_{100} value of 10.98 nm, which is corresponding to a large unit cell parameter (a_0) of 12.68 nm. Grafting the CPTMS and H-acid to the SBA-15 in two subsequent steps resulted in slightly shift of (100) peak to higher 2θ values, and therefore the SBA-15-Cl and SBA-15-HA materials show lower d_{100} and a_0 .

It is also observed that the pore volume and specific surface area of SBA-15 dramatically shrank during the first step of modification, and the final step of modification did not cause a significant decrease of pore volume and specific surface area of studied materials. Considering the unit-cell parameter and pore diameter, the wall thickness of materials can be calculated by subtracting of d_p from a_0 . It increased from 5.63 nm in SBA-15 to 7.52 and 7.64 nm in SBA-15-Cl and SBA-15-HA, respectively. On the basis of the above-discussed observations, it can be concluded that CPTMS and H-acid into SBA-15 took place inside the SBA-15 channels and on its wall surface.

3.2. FT-IR Spectroscopy. The FT-IR spectroscopy was used to verify the insertion of CPTMS and H-acid into the SBA-15 structure. Figure 3 shows the FT-IR spectra of SBA-15, SBA-15-Cl

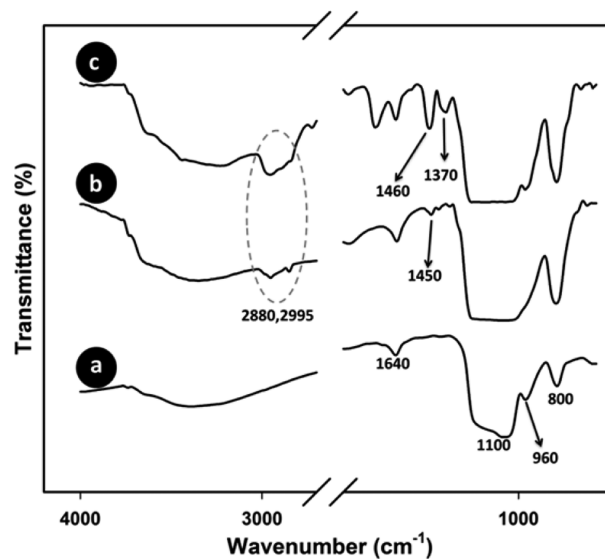


Figure 3. FT-IR spectra of (a) SBA-15, (b) SBA-15-Cl, and (c) SBA-15-HA.

and SBA-15-HA. The SBA-15 represents two major peaks around 800 and 1100 cm^{-1} which are attributed to the Si–O–Si framework stretching vibrations. The observed band around 1640 cm^{-1} can be related to vibrations of physically adsorbed water molecules. The successful incorporation of CPTMS into the SBA-15 after the first

modification step was examined by comparison of FT-IR spectrum of SBA-15 and SBA-15-Cl. The vibrations of $\text{CH}_2\text{--Cl}$ groups normally should exhibit two major peaks around 800 and 1200 cm^{-1} , but overlapping with $\text{Si}\text{--O}\text{--Si}$ bands prevents unambiguous observation of these bands.

The observed bands at 1450, 2880, and 2995 cm^{-1} are assigned to scissoring, symmetric stretching, and asymmetric stretching of $-\text{CH}_2-$ groups. The presence of mentioned peaks confirms that CPTMS successfully inserted to the SBA-15 material. The attachment of H-acid to the SBA-15-Cl during the final step of modification was also confirmed by observing some characteristic peaks. Although some important peaks cannot be resolved due to the overlap with broad bands of $\text{Si}\text{--O}\text{--Si}$ framework, there are other resolved peaks which still can confirm successful modification reaction which was done. The present bands at 1460 and 1640 cm^{-1} can be related to $\text{C}=\text{C}$ stretching in aromatic rings. The former strong band overlaps with weak band related to $-\text{CH}_2-$ scissoring vibration. The observed band around 1370 cm^{-1} was attributed to asymmetric stretching of S=O bonds of sulfonate groups. The other observed band for SBA-15-HA is the one present at around 1700 cm^{-1} that can be assigned to $-\text{NH}-$ bending.

3.3. Thermogravimetry Analysis. Figure 4 shows the TGA curves of SBA-15-Cl and SBA-15-HA materials that can be used

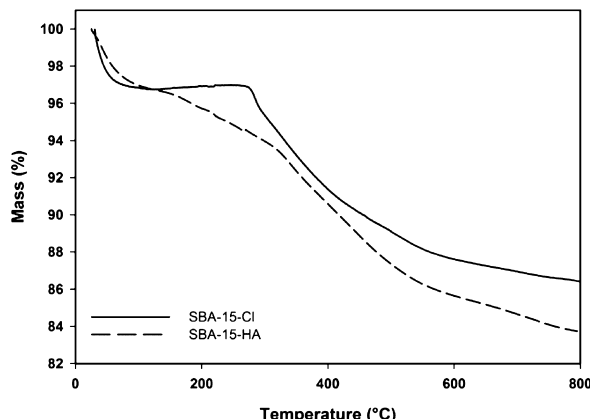


Figure 4. TGA curves of SBA-15-Cl and SBA-15-HA.

for calculation of the approximate loaded amount of organic moieties. Both curves show an initial mass loss due to removal of physically adsorbed water and other volatiles. Then, the major mass loss occurs which corresponds to elimination of organic moieties. Finally, the gradual dehydroxylation of $\text{Si}\text{--OH}$ groups can be responsible for the small weight loss above $600 \text{ }^{\circ}\text{C}$. TGA curves show the major mass loss of $\sim 11\%$ and $\sim 10\%$ for SBA-15-Cl and SBA-15-HA, respectively. Therefore, the approximate amount of present organic moieties in SBA-15-Cl and SBA-15-HA is calculated to be 1.43 and 0.3 mmol/g, respectively. Actually, as the reaction between SBA-15-Cl and H-acid is not complete, there are still unreacted chloropropyl groups in SBA-15-HA, and then the obtained amount of organic moiety in SBA-15-HA is an overestimated value of H-acid moiety.

3.4. Optical Sensing Properties. The fluorescence spectroscopy was used for testing the recognition ability of SBA-15-HA material for optical sensing. The fluorescence response of SBA-15-HA toward addition of various metal ions was recorded at 415 nm following excitation at 340 nm . Figure 5 illustrates the quenching ratio, $((F_0 - F)/F_0)$, of fluorescence intensity upon addition of $1 \times 10^{-4} \text{ M}$ solution of common interfering metal ions (Li^+ , Na^+ , K^+ , Ag^+ , Ca^{2+} , Mg^{2+} , Al^{3+} , Mn^{2+} , Cr^{3+} , Co^{2+} , Ni^{2+} , Cu^{2+} , Cd^{2+} , Zn^{2+} , Pb^{2+} , and Hg^{2+}) to SBA-15-HA suspension (0.05 g mL^{-1}) at pH ~ 7.0 . It has been reported previously that pH 6.0–7.0 satisfies the fast and sensitive fluorescence response of H-acid besides the suitability for environmental and biological applications. It is also worth noting that the protective effect of SBA-15 network against pH variation enables the performing of measurements without using buffer solutions. Figure 5 shows that the fluorescence intensity of SBA-15-HA dramatically decreased by addition of Hg^{2+} in comparison with other cations which did not produce significant quenching of fluorescence intensity. It means that the SBA-15-HA exhibits high selectivity to Hg^{2+} . It can be related to stronger attraction between Hg^{2+} ions and sulfonate groups of grafted H-acid molecules to the SBA-15. Therefore, a metal–organic complex is formed that changes the electronic structure of the H-acid and significantly decreases the fluorescence intensity. For the other tested metal ions it can be proposed that either there is no considerable fluorophore–metal ion interaction or the formed complex does not differ in emission from the H-acid significantly.

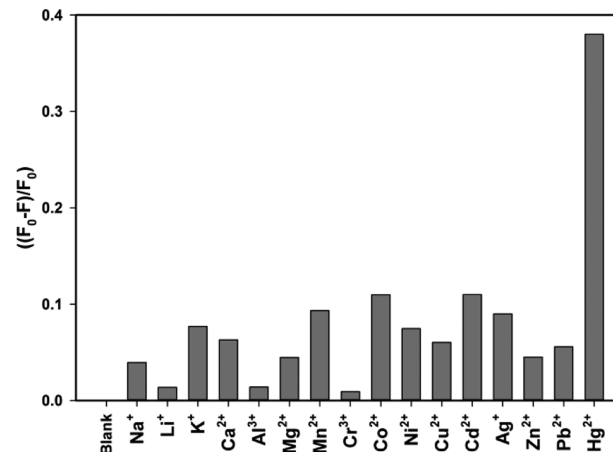


Figure 5. Quenching ratio $((F_0 - F)/F_0)$ of fluorescence response of SBA-15-HA aqueous dispersion (0.05 g mL^{-1}) in the presence of various metal ions at pH 7.0 ($\lambda_{\text{exc}} = 340 \text{ nm}$, $\lambda_{\text{emi}} = 415 \text{ nm}$).

Pb^{2+} , and Hg^{2+}) to SBA-15-HA suspension (0.05 g mL^{-1}) at pH ~ 7.0 . It has been reported previously that pH 6.0–7.0 satisfies the fast and sensitive fluorescence response of H-acid besides the suitability for environmental and biological applications. It is also worth noting that the protective effect of SBA-15 network against pH variation enables the performing of measurements without using buffer solutions. Figure 5 shows that the fluorescence intensity of SBA-15-HA dramatically decreased by addition of Hg^{2+} in comparison with other cations which did not produce significant quenching of fluorescence intensity. It means that the SBA-15-HA exhibits high selectivity to Hg^{2+} . It can be related to stronger attraction between Hg^{2+} ions and sulfonate groups of grafted H-acid molecules to the SBA-15. Therefore, a metal–organic complex is formed that changes the electronic structure of the H-acid and significantly decreases the fluorescence intensity. For the other tested metal ions it can be proposed that either there is no considerable fluorophore–metal ion interaction or the formed complex does not differ in emission from the H-acid significantly.

The recognition ability of SBA-15-HA for Hg^{2+} ions as well as their complexation was examined by performing fluorescence titration. Microliter portions of Hg^{2+} solution gradually were added to the aqueous suspension of SBA-15-HA (0.05 g mL^{-1}) at pH 7.0 excited at 340 nm , and the emission spectra of SBA-15-HA varying with Hg^{2+} concentration were recorded until no more quenching was observed (Figure 6).

Figure 7 shows the plot of F_0/F versus $[\text{Hg}^{2+}]$ with a good linear relationship between relative fluorescence intensity and quencher concentration range of 3.3×10^{-7} to $5 \times 10^{-6} \text{ M}$ following the equation $F_0/F = 1.22 \times 10^5 [\text{Hg}^{2+}] + 0.99$ with regression coefficient (r^2) of 0.99.

Considering the Stern–Volmer equation³⁵ (eq 1), the Stern–Volmer quenching constant (K_{SV}) is $1.22 \times 10^5 \text{ M}^{-1}$.

$$\frac{F_0}{F} = 1 + K_{\text{SV}}[\text{Q}] \quad (1)$$

where F_0 is fluorescence intensity of SBA-15-HA suspension without addition of Hg^{2+} , F is fluorescence intensity of SBA-15-HA suspension after addition of various concentration of Hg^{2+} solution, and K_{SV} is Stern–Volmer quenching constant. The detection limit (DL) was calculated from eq 2:

$$\text{DL} = \frac{K_{\text{SV}}}{m} \quad (2)$$

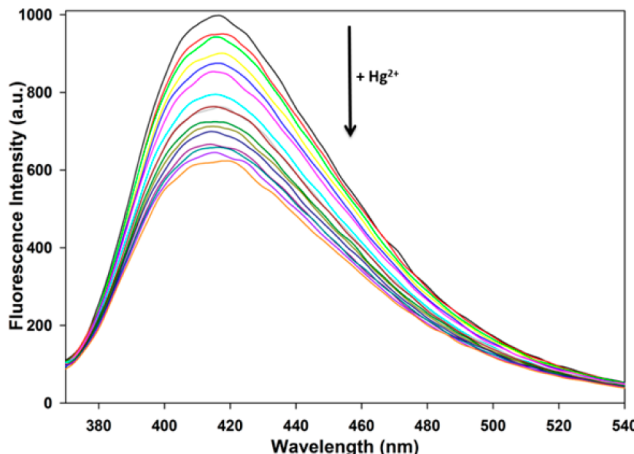


Figure 6. Fluorescence spectra changes of SBA-15-HA aqueous suspension (0.05 g mL^{-1}) upon addition of different Hg^{2+} concentrations at pH 7.0 ($\lambda_{\text{exc}} = 340 \text{ nm}$, $\lambda_{\text{emi}} = 415 \text{ nm}$).

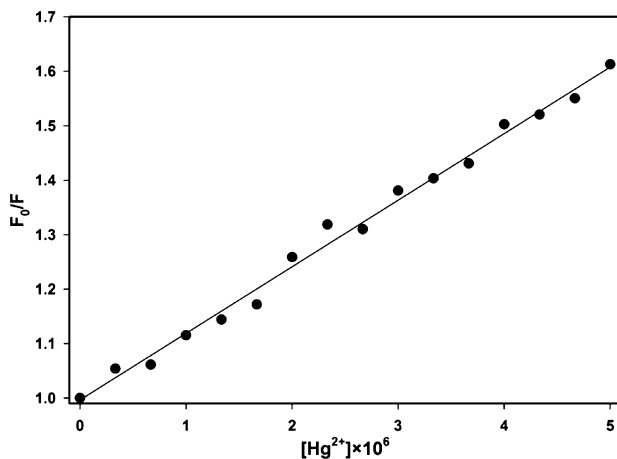


Figure 7. Stern–Volmer plot of SBA-15-HA aqueous suspension (0.05 g mL^{-1}) upon addition of different Hg^{2+} concentrations at pH 7.0 ($\lambda_{\text{exc}} = 340 \text{ nm}$, $\lambda_{\text{emi}} = 415 \text{ nm}$).

where K is the confidence level that is generally set to 3, S_d is standard deviation of blank, and m is the slope of $F_0 - [\text{Hg}^{2+}]$ plot. Herein, S_d and m are calculated to be 4.9 and 7×10^7 , respectively. Then, the absolute detection limit is calculated to be $2.1 \times 10^{-7} \text{ M}$.

As is observed in Figure 6, the fluorescence intensity of SBA-15-HA was not completely quenched by addition of Hg²⁺ solution. Qualitatively, it can be related to the presence of fluorescent molecules inside the channels of SBA-15 that make them inaccessible to Hg²⁺ ion. In such cases the modified Stern–Volmer equation (eq 3) can be applied for quantitative evaluation of the accessible fraction of fluorophore molecules.³⁶

$$\frac{F_0}{F_0 - F} = \frac{1}{f_a K_a [Q]} + \frac{1}{f_a} \quad (3)$$

where f_a is the fraction of initial fluorophores that is accessible to quencher and K_a is Stern–Volmer quenching constant of the accessible fraction. Plotting of $F_0/(F_0 - F)$ versus $1/[Q]$ provides $1/f_a$ as intercept and $1/f_a K_a$ as slope. Thus, f_a is obtained as 0.53 from a modified Stern–Volmer plot (Figure 8) reveals that almost more than half of fluorophores are accessible to Hg²⁺ ions. It can be taken into account as the rationalized reason for the remaining observed fluorescence.

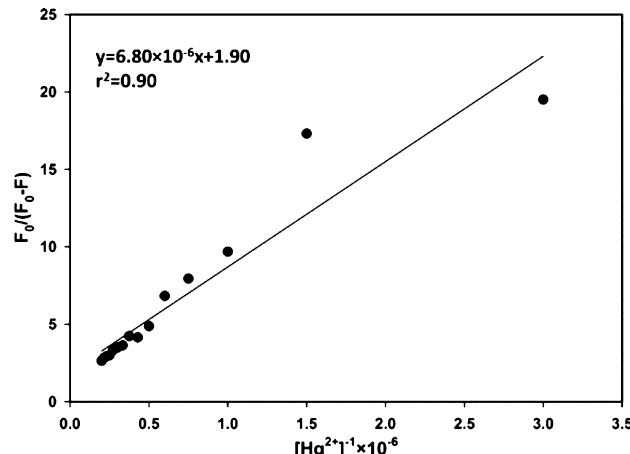


Figure 8. Modified Stern–Volmer plot of SBA-15-HA aqueous suspension (0.05 g mL^{-1}) upon addition of different Hg^{2+} concentrations at pH 7.0 ($\lambda_{\text{exc}} = 340 \text{ nm}$, $\lambda_{\text{emi}} = 415 \text{ nm}$).

An important issue in fluorescent sensors is the mechanism of quenching or enhancement of fluorescence intensity. Here, we intend to rationalize the quenching process in H-acid/Hg system. Since emission is radiative relaxation of excited molecules, UV–vis spectra of H-acid with addition of Hg²⁺ were recorded (Figure 9a). It is observed that the UV–vis spectrum of H-acid shows one broad peak centered at $\sim 340 \text{ nm}$. Addition of Hg²⁺ and subsequent interaction between Hg²⁺ and H-acid resulted in diminishing of the absorbance of the mentioned peak and establishment of new peak at $\sim 430 \text{ nm}$. As reported previously by Young,²³ this observation can superficially be considered as a reason for fluorescence quenching. It reveals that the high energy band still exists and a new low-energy band forms. Therefore, the altering of H-acid electronic structure of H-acid by interacting with Hg²⁺ can be considered responsible for fluorescence quenching. For providing further proof, the UV–vis spectra of H-acid with addition of Cd²⁺ and Zn²⁺ (as counterexamples) were also recorded (Figure 9b). In the case of Zn²⁺ addition, no significant change is observed; however, for Cd²⁺ a blue-shift in the broad peak is observed. This means that probably the aforementioned observed changes in UV–vis spectra of [H-acid]Hg²⁺ can be taken into account for the fluorescence quenching. Looking more closely at the H-acid and [H-acid]–Hg²⁺ complex, computational studies were carried out in order to obtain more detailed information on structure, bonding, and electronic transitions in H-acid and [H-acid]Hg²⁺.

3.5. Structure, Bonding, and Quenching Mechanism.

Young²³ suggested that each Hg²⁺ interacts with two oxygen atoms of sulfonate moieties in H-acid. Sun et al.²⁴ have done a computational effort to rationalize the [H-acid]Hg²⁺ structure and obtained a similar structure to the one suggested by Young.²³ Herein, we employed aug-cc-pVDZ-PP basis set along with its corresponding effective core potential (ECP) in order to let the molecule be optimized more accurately. Optimized structures (see Supporting Information Figures S1 and S2) show that [H-acid]Hg²⁺ complex relaxed to a different structure rather than previously reported by Sun et al.²⁴ Herein, each of Hg²⁺ ions interact with one of oxygen atoms of sulfonate groups and as the Hg²⁺ ions usually form two coordinated complexes the second coordination site can be filled by water molecules. The Cartesian coordinates of optimized structures are provided in Tables S2–S4.

The Mayer bond orders (MBO)³⁷ of [H-acid]Hg²⁺ complex were calculated (see Table S5) and used for obtaining a better

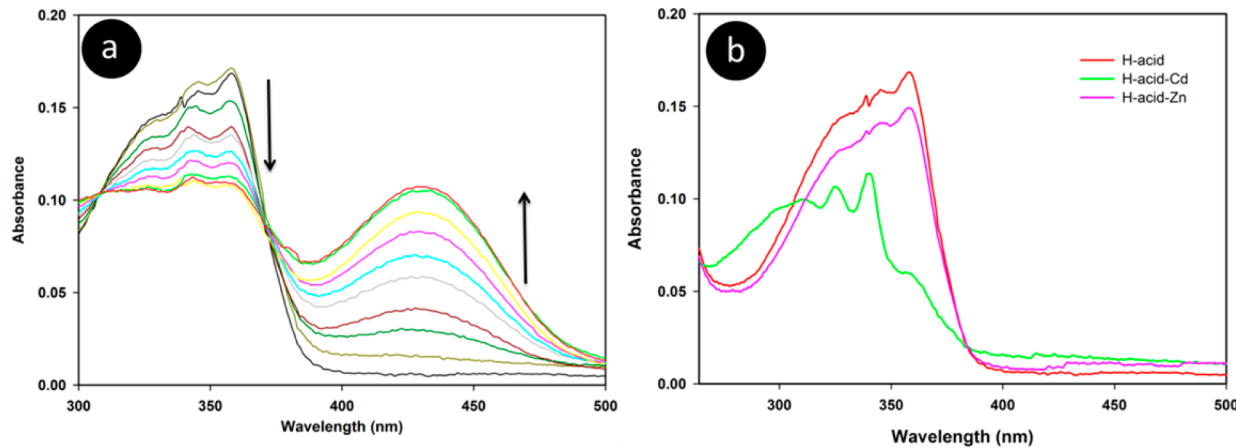


Figure 9. UV-vis spectra of H-acid (a) upon addition of different Hg^{2+} concentrations and (b) upon addition of Zn^{2+} and Cd^{2+} .

insight into the interaction and bonding of H-acid and Hg^{2+} . In order to have a rationalized interpretation of MBOs for $\text{Hg}-\text{O}$ bonds, MBO of well-known bonds such as C–C, C–N, and C–O are discussed. It is observed that although C–C bonds took different MBO values, the average MBO is obtained as 1.38 that is in consistent with resonance structure of naphthyl moiety. Additionally, C–N and C–O bonds which are single covalent bonds have MBO of equal to unity. Then, the $\text{Hg}-\text{O}$ bonds show the MBO value of 0.67 that can be indicative for the presence of a significant interaction between Hg and O. As the MBO is less than unity it can be proposed that the interaction is mixture of ionic and covalent bonding.

The selected bond lengths are presented in Table 2. The C–S bonds did not change significantly upon coordination of Hg^{2+} to

Table 2. Selected Bond Lengths Calculated in Aqueous Solution at the PBE0/6-31++G PCM Level of Theory (aug-cc-pVDZ-PP Basis Set along with Its Corresponding ECP Used for Hg)^a**

H-acid		[H-acid] Hg^{2+}	
selected bond	bond length (Å)	selected bond	bond length (Å)
S1–C6	1.789	S1–C1	1.781
S2–C9	1.788	S2–C2	1.783
S1–O2	1.479	S1–O2	1.472
S1–O3	1.495	S1–O3	1.542
S1–O4	1.492	S1–O4	1.469
S2–O5	1.479	S2–O5	1.472
S2–O6	1.491	S2–O6	1.543
S2–O7	1.494	S2–O7	1.470
O3–Hg1		O3–Hg1	2.179
O6–Hg2		O6–Hg2	2.177

^aFor atom numbers and labels see Figures S1 and S2.

H-acid. The Hg^{2+} ions coordinated to H-acid through O3 and O6 oxygen atoms. The bond lengths are similar and 2.179 and 2.177 Å for Hg1–O3 and Hg2–O6 bonds, respectively. It is observed that the S1–O3 and S2–O6 bonds elongated and two other oxygen–sulfur bonds shortened in [H-acid] Hg^{2+} (for atom numbers and labels see Figures S1 and S2).

It can be suggested that when the Hg^{2+} interacts with O3 or O6 atoms, the localized electron density on sulfonate groups is polarized toward Hg^{2+} ions. On one hand, the shared electrons between interacting oxygen atoms and Hg^{2+} ions get closer to oxygen atoms, and then the corresponding S–O bonds weaken and elongate. On the other hand, the sulfur atoms attracted more

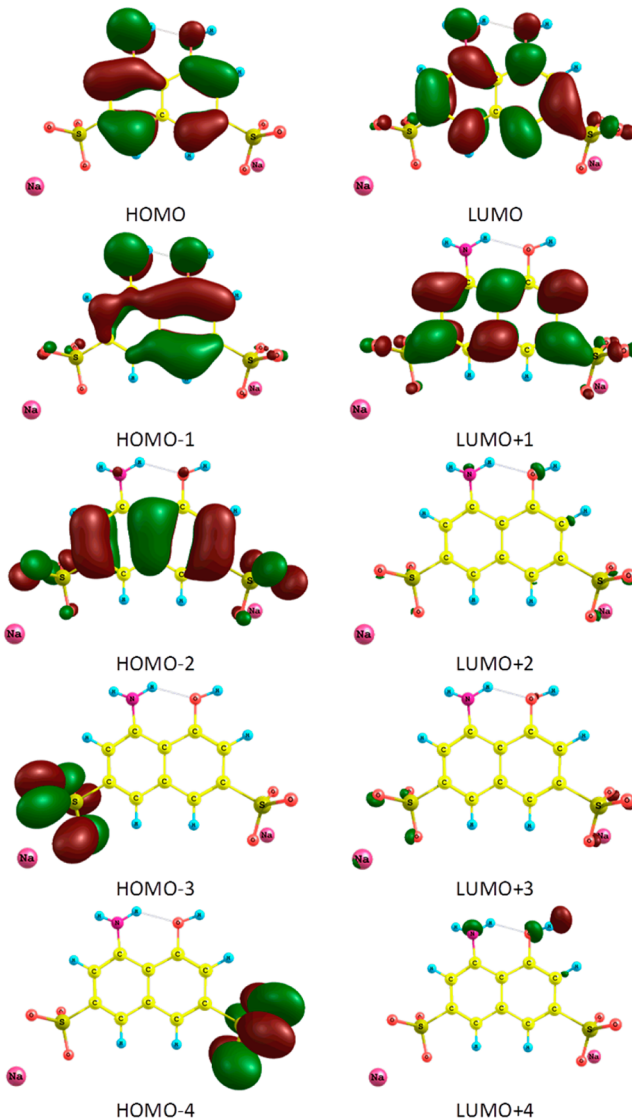


Figure 10. Frontier molecular orbitals for H-acid calculated in aqueous solution at the PBE0/6-31++G** PCM level of theory (isosurface value = 0.02 e/Å³).

electron density from two other oxygen atoms which caused the other bonds to become stronger and therefore shortened.

Table 3. Electronic Transitions of H-acid and $[H\text{-acid}]Hg^{2+}$ Calculated in Aqueous Solution at the PBE0/6-31++G PCM Level of Theory (aug-cc-pVDZ-PP Basis Set along with Its Corresponding ECP Used for Hg)**

electronic transitions	composition	CI	energy/eV (λ/nm)	f
$S_0 \rightarrow S_1$	HOMO-2 \rightarrow LUMO	0.1895	3.80 (326.2)	0.2182
	HOMO \rightarrow LUMO	-0.1416		
	HOMO \rightarrow LUMO+1	0.6625		
$S_0 \rightarrow S_1$	$[H\text{-acid}]Hg^{2+}$			
	HOMO \rightarrow LUMO	0.3012	2.1839 (567.71)	0.0185
$S_0 \rightarrow S_4$	HOMO \rightarrow LUMO+1	0.6387	3.7557 (330.12)	0.1397
	HOMO-3 \rightarrow LUMO+1	-0.1661		
	HOMO-2 \rightarrow LUMO+1	0.1857		
	HOMO-2 \rightarrow LUMO+2	0.1424		
	HOMO-1 \rightarrow LUMO	0.2541		
	HOMO-1 \rightarrow LUMO+1	-0.1491		
	HOMO \rightarrow LUMO+2	0.1485		
	HOMO \rightarrow LUMO+3	0.5440		

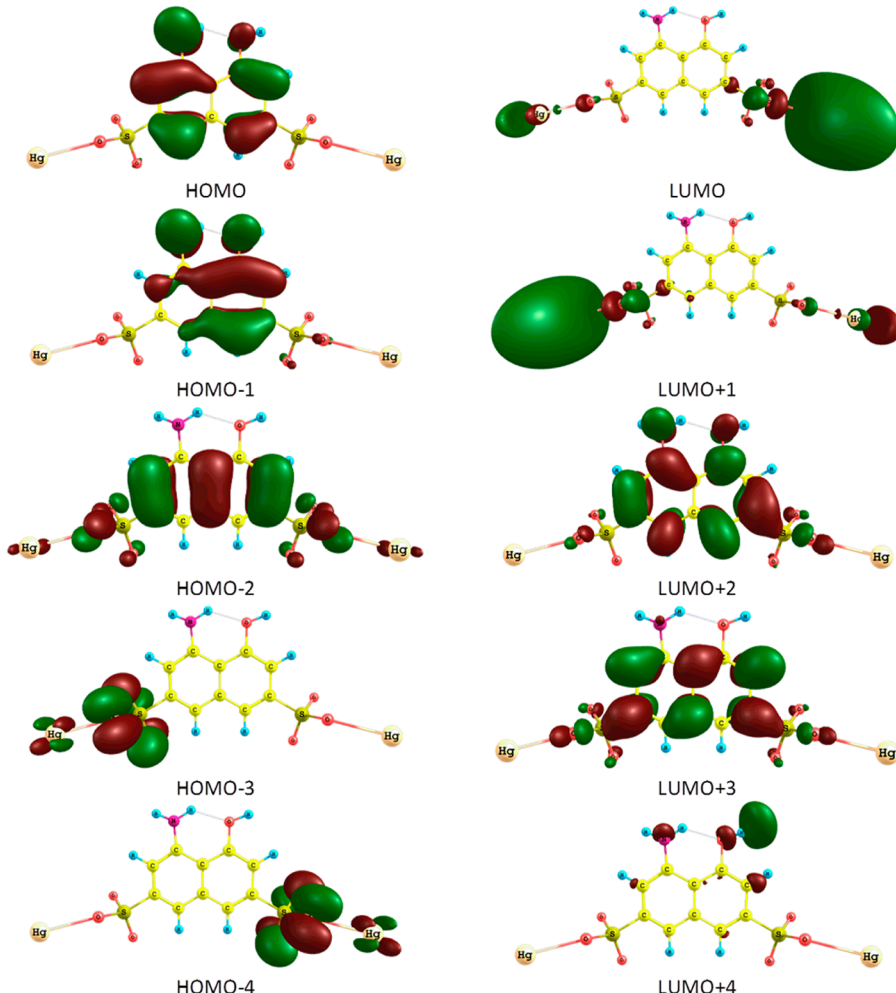


Figure 11. Frontier molecular orbitals for $[H\text{-acid}]Hg^{2+}$ calculated in aqueous solution at the PBE0/6-31++G** PCM level of theory (aug-cc-pVDZ-PP basis set along with its corresponding ECP used for Hg) (isosurface value = 0.02 e/ \AA^3).

In order to find an explanation for fluorescence quenching, electronic spectrum of H-acid and $[H\text{-acid}]Hg^{2+}$ were simulated, and the results are presented in Table 3. The lowest-lying excited state ($S_0 \rightarrow S_1$) of H-acid corresponds to excitation energy of 326.2 nm (3.80 eV) and is allowed considering the oscillator strength (*f*) and overlapping of HOMO to LUMO+1, which is the main transition found with configuration interaction (CI) coefficient of 0.6625.

According to MO isosurfaces (Figure 10), it is obvious that HOMO and LUMO+1 are more localized on the naphthalene ring and therefore electron transition is allowed. This reveals that the reverse transition, i.e., $S_1 \rightarrow S_0$, is also allowed, and therefore the H-acid can be considered as a fluorescent material.³⁸ For $[H\text{-acid}]Hg^{2+}$, the lowest-lying excited state exhibits a much longer excitation wavelength of 567.71 nm with small oscillator strength of 0.0185.

This small f value, besides the lack of overlapping for HOMO and LUMO/LUMO+1 (Figure 11), shows that the excitation of the molecule to its lowest-lying excited state is forbidden; however, it can be populated by internal conversion (IC) process from the higher excited states. The first low-lying allowed transition is $S_0 \rightarrow S_4$ with excitation energy of 330.12 nm (3.76 eV) and f value of 0.1397. It is worth noting that according to energy and shape of LUMO and LUMO+1 (-3.18 and -3.17 eV, respectively) they are degenerated excited states, and they are both localized on the SO_3-Hg moieties of the complex; therefore, it is reasonable to assume that electron transfer to each of them has an equal opportunity. Then, it is possible that the excited electron to S_4 excited state returns to the lowest excited states such as S_1 and S_2 by IC process. This means that when the excited electron from S_4 excited states relaxes to lower-lying excited states, both S_1 and S_2 states can be populated with equal probability. Based on Kasha's rule about the IC process, it occurs very fast and in nonradiative manner. Thus, relaxation from S_4 to S_1 or S_2 takes place before any other relaxation process. Finally, as it was mentioned above that the $S_0 \rightarrow S_1$ is forbidden in $[\text{H-acid}]\text{Hg}^{2+}$ complex; therefore, the relaxation from S_1 to S_0 is also not allowed, and S_1 is a dark state. Consequently, the excited molecule returns to ground state through a nonradiative path and it shows itself as a quench in fluorescence.

For providing a quantitative insight on fluorescence quenching and nonradiative relaxation in $[\text{H-acid}]\text{Hg}^{2+}$, the radiative lifetime (τ , ns) of H-acid and $[\text{H-acid}]\text{Hg}^{2+}$ were calculated for spontaneous emission using Einstein transition probabilities according to eq 4:³⁸

$$\tau = \frac{c^3}{2E^2f} \quad (4)$$

where c is the speed of light in vacuum, E is the transition energy, and f is the oscillator strength (all in atomic units). The calculated radiative lifetimes for H-acid and $[\text{H-acid}]\text{Hg}^{2+}$ using the presented data in Table 3 are 7.3 and 262 ns, respectively. Fundamentally, the efficiency of light emission decreases with increasing the radiative lifetime due to higher probability for nonradiative relaxation. The H-acid first singlet excited state likewise other organic molecules is emissive when the radiative lifetime lies below 10 ns but complexation of Hg to H-acid significantly increases the radiative lifetime and less emission is observed.

Up to this point, a quenching mechanism in the $[\text{H-acid}]\text{Hg}^{2+}$ system was proposed based on the experimental observations and theoretical calculations. However, there is still an unanswered doubt regarding the origin of a new formed band at 430 nm in UV-vis spectra of $[\text{H-acid}]\text{Hg}^{2+}$. Since no related electronic transition was observed in singlet-singlet transitions, singlet-triplet transitions were also calculated for $[\text{H-acid}]\text{Hg}^{2+}$. Interestingly, a singlet-to-triplet electronic transition was observed at 418 nm. It is worth noting that generally singlet-to-triplet transition is spin forbidden and cannot be observed. However, due to the presence of heavy Hg atoms in the complex, spin-orbit coupling can take place. Therefore, singlet and triplet states are mixed, and consequently the spin-forbidden nature is diminished and triplet state can participate in both absorption and emission.³⁹

4. CONCLUSION AND FUTURE PROSPECTS

Concluding, we have synthesized the SBA-15 nanoporous silica with the H-acid dye intermediate in a two-step modification approach and unambiguously characterized the synthesized

materials by means of various techniques such as SAXS, N₂ adsorption-desorption measurements, etc. The interpretation of characterization data showed that the H-acid successfully grafted to the SBA-15 and the final product structure preserved after two steps of modifications and showing high specific surface area and accessible open pores, which makes it applicable for further applications. The SBA-15-HA ability for fluorescent sensing of metal ions examined and presented a high selectivity toward Hg^{2+} among various metal ions. The computational studies helped us to go further in determination of $[\text{H-acid}]\text{Hg}^{2+}$ structure and electronic structure. Therefore, a rationalized mechanism for fluorescence quenching was proposed showing that the interaction between H-acid and Hg^{2+} ions altered the electronic structure of H-acid and converted its emissive lowest-lying excited state to a dark state that it has been observed as fluorescence quenching.

Grafting the H-acid into other mesoporous silicas such as MCM-41, MCM-48, SBA-16, etc., is proposed to study the effect of support structure and pore diameter on the sensing properties of such materials. Simulation of emission spectra that needs the optimization of excited states as well as examination of other DFT methods on electronic structures of H-acid and $[\text{H-acid}]\text{Hg}^{2+}$ is needed and is currently under study within our research group.

■ ASSOCIATED CONTENT

S Supporting Information

Optimized structure of H-acid and $[\text{H-acid}]\text{Hg}^{2+}$; table of Mayer bond orders; table of Cartesian coordinates of H-acid and $[\text{H-acid}]\text{Hg}^{2+}$ optimized structures in gas phase and aqueous media. This material is available free of charge via the Internet at <http://pubs.acs.org>.

■ AUTHOR INFORMATION

Corresponding Author

*Fax +98 21 6111 3301; e-mail abadie@khayam.ut.ac.ir (A.B.).

Notes

The authors declare no competing financial interest.

■ ACKNOWLEDGMENTS

The authors thank the research council of University of Tehran for financial support. J.B.F. is also thankful to DGTIC-UNAM for granting access to their supercomputing facilities known as Kan Balam. P.Z. also thanks Dr. Cina Foroutan-Nejad for his valuable help.

■ REFERENCES

- Zhao, D.; Feng, J.; Huo, Q.; Melosh, N.; Fredrickson, G. H.; Chmelka, B. F.; Stucky, G. D. Triblock Copolymer Syntheses of Mesoporous Silica with Periodic 50 to 300 Angstrom Pores. *Science* **1998**, *279*, 548–552.
- Zhao, D.; Huo, Q.; Feng, J.; Chmelka, B. F.; Stucky, G. D. Nonionic Triblock and Star Diblock Copolymer and Oligomeric Surfactant Syntheses of Highly Ordered, Hydrothermally Stable, Mesoporous Silica Structures. *J. Am. Chem. Soc.* **1998**, *120*, 6024–6036.
- Gao, L.; Wang, Y.; Wang, J.; Huang, L.; Shi, L.; Fan, X.; Zou, Z.; Yu, T.; Zhu, M.; Li, Z. A Novel Zn^{II}-Sensitive Fluorescent Chemosensor Assembled within Aminopropyl-Functionalized Mesoporous SBA-15. *Inorg. Chem.* **2006**, *45*, 6844–6850.
- Bin, F.; Song, C.; Lv, G.; Song, J.; Cao, X.; Pang, H.; Wang, K. Structural Characterization and Selective Catalytic Reduction of Nitrogen Oxides with Ammonia: A Comparison between Co/ZSM-5 and Co/SBA-15. *J. Phys. Chem. C* **2012**, *116*, 26262–26274.

- (5) Wang, X.; Lin, K. S. K.; Chan, J. C. C.; Cheng, S. Direct Synthesis and Catalytic Applications of Ordered Large Pore Aminopropyl-Functionalized SBA-15 Mesoporous Materials. *J. Phys. Chem. B* **2005**, *109*, 1763–1769.
- (6) Zarabadi-Poor, P.; Badiei, A. Synthesis of Carbon Nanotubes Using Metal-Modified Nanoporous Silicas. In *Carbon Nanotubes—Growth and Applications*; Naraghi, M., Ed.; InTech: Rijeka, 2011; pp 59–74.
- (7) Hashemi, P.; Shamizadeh, M.; Badiei, A.; Zarabadi-Poor, P.; Ghiasvand, A. R.; Yarahmadi, A. Amino Ethyl-Functionalized Nanoporous Silica as a Novel Fiber Coating for Solid-Phase Microextraction. *Anal. Chim. Acta* **2009**, *646*, 1–5.
- (8) Wang, Y.; Li, B.; Zhang, L.; Liu, L.; Zuo, Q.; Li, P. A Highly Selective Regenerable Optical Sensor for Detection of Mercury(II) Ion in Water using Organic-Inorganic Hybrid Nanomaterials Containing Pyrene. *New J. Chem.* **2010**, *34*, 1946–1953.
- (9) Fryxell, G. E. The Synthesis of Functional Mesoporous Materials. *Inorg. Chem. Commun.* **2006**, *9*, 1141–1150.
- (10) Rurack, K.; Kollmannsberger, M.; Resch-Genger, U.; Daub, J. A Selective and Sensitive Fluoroionophore for Hg^{II}, AgI, and Cu^{II} with Virtually Decoupled Fluorophore and Receptor Units. *J. Am. Chem. Soc.* **2000**, *122*, 968–969.
- (11) Mason, W. T. *Fluorescence and Luminescent Probes for Biological Activity*; Academic Press: San Diego, 1999.
- (12) Balaji, T.; El-Safty, S. A.; Matsunaga, H.; Hanaoka, T.; Mizukami, F. Optical Sensors Based on Nanostructured Cage Materials for the Detection of Toxic Metal Ions. *Angew. Chem.* **2006**, *118*, 7360–7366.
- (13) Jin, Z.; Zhang, X.-B.; Xie, D.-X.; Gong, Y.-J.; Zhang, J.; Chen, X.; Shen, G.-L.; Yu, R.-Q. Clicking Fluoroionophores onto Mesoporous Silicas: A Universal Strategy toward Efficient Fluorescent Surface Sensors for Metal Ions. *Anal. Chem.* **2010**, *82*, 6343–6346.
- (14) Dong, Z.; Dong, Z.; Wang, P.; Tian, X.; Geng, H.; Li, R.; Ma, J. A Fluorescent Probe for Zinc Detection Based on Organically Functionalized SBA-15. *Appl. Surf. Sci.* **2010**, *257*, 802–806.
- (15) Zhang, N.; Li, G.; Cheng, Z.; Zuo, X. Rhodamine B Immobilized on Hollow Au–HMS Material for Naked-Eye Detection of Hg²⁺ in Aqueous Media. *J. Hazard. Mater.* **2012**, *229–230*, 404–410.
- (16) Kim, H. J.; Lee, S. J.; Park, S. Y.; Jung, J. H.; Kim, J. S. Detection of Cu^{II} by a Chemodosimeter-Functionalized Monolayer on Mesoporous Silica. *Adv. Mater.* **2008**, *20*, 3229–3234.
- (17) Ros-Lis, J. V.; Casasús, R.; Comes, M.; Coll, C.; Marcos, M. D.; Martínez-Máñez, R.; Sancenón, F.; Soto, J.; Amorós, P.; Haskouri, J. E.; et al. A Mesoporous 3D Hybrid Material with Dual Functionality for Hg²⁺ Detection and Adsorption. *Chem.—Eur. J.* **2008**, *14*, 8267–8278.
- (18) Zhang, N.; Li, G.; Zhao, J.; Liu, T. Three-Dimensional Wormhole Mesoporous-Based Material as a Regenerative Solid Optical Sensor for Detection of Hg²⁺ in Aqueous Media. *New J. Chem.* **2013**, *37*, 458–463.
- (19) Onyido, I.; Norris, A. R.; Buncel, E. Biomolecule–Mercury Interactions: Modalities of DNA Base–Mercury Binding Mechanisms. Remediation Strategies. *Chem. Rev.* **2004**, *104*, 5911–5930.
- (20) Zhou, P.; Meng, Q.; He, G.; Wu, H.; Duan, C.; Quan, X. Highly Sensitive Fluorescence Probe Based on Functional SBA-15 for Selective Detection of Hg²⁺ in Aqueous Media. *J. Environ. Monit.* **2009**, *11*, 648–653.
- (21) Song, C.; Zhang, X.; Jia, C.; Zhou, P.; Quan, X.; Duan, C. Highly Sensitive and Selective Fluorescence Sensor Based on Functional SBA-15 for Detection of Hg²⁺ in Aqueous Media. *Talanta* **2010**, *81*, 643–649.
- (22) Meng, Q.; Zhang, X.; He, C.; Zhou, P.; Su, W.; Duan, C. A Hybrid Mesoporous Material Functionalized by 1,8-Naphthalimide-Base Receptor and the Application as Chemosensor and Absorbent for Hg²⁺ in Water. *Talanta* **2011**, *84*, 53–59.
- (23) Young, S. Selective Fluorescent Hg(II) Detection in Aqueous Solutions with a Dye Intermediate. *Spectrochim. Acta, Part A* **2007**, *68*, 705–709.
- (24) Sun, Z.; Jin, L.; Zhang, S.; Shi, W.; Pu, M.; Wei, M.; Evans, D. G.; Duan, X. An Optical Sensor Based on H-acid/Layered Double Hydroxide Composite Film for the Selective Detection of Mercury Ion. *Anal. Chim. Acta* **2011**, *702*, 95–101.
- (25) Zarabadi-Poor, P.; Badiei, A.; Fahlman, B. D.; Arab, P.; Mohammadi Ziarani, G. One-Pot Synthesis of Ethanolamine-Modified Mesoporous Silica. *Ind. Eng. Chem. Res.* **2011**, *50*, 10036–10040.
- (26) Frisch, M. J.; Trucks, G. W.; Schlegel, H. B.; Scuseria, G. E.; Robb, M. A.; Cheeseman, J. R.; Scalmani, G.; Barone, V.; Mennucci, B.; Petersson, G. A.; et al. *Gaussian 09, Revision B.01*; Gaussian, Inc.: Wallingford, CT, 2009.
- (27) Adamo, C.; Barone, V. Toward Reliable Density Functional Methods without Adjustable Parameters: The PBE0Model. *J. Chem. Phys.* **1999**, *110*, 6158–6170.
- (28) Frantl, M. M.; Pietro, W. J.; Hehre, W. J.; Binkley, J. S.; Gordon, M. S.; DeFrees, D. J.; Pople, J. A. Self-Consistent Molecular Orbital Methods. XXIII. A Polarization-Type Basis Set for Second-Row Elements. *J. Chem. Phys.* **1982**, *77*, 3654–3665.
- (29) Hariharan, P. C.; Pople, J. A. The Influence of Polarization Functions on Molecular Orbital Hydrogenation Energies. *Theor. Chim. Acta* **1973**, *28*, 213–222.
- (30) Figgen, D.; Rauhut, G.; Dolg, M.; Stoll, H. Energy-Consistent Pseudopotentials for Group 11 and 12 Atoms: Adjustment to Multi-configuration Dirac–Hartree–Fock Data. *Chem. Phys.* **2005**, *311*, 227–244.
- (31) Peterson, K. A.; Puzzarini, C. Systematically Convergent Basis Sets for Transition Metals. II. Pseudopotential-based Correlation Consistent Basis Sets for the Group 11 (Cu, Ag, Au) and 12 (Zn, Cd, Hg) Elements. *Theor. Chem. Acc.* **2005**, *114*, 283–296.
- (32) Tomasi, J.; Mennucci, B.; Cammi, R. Quantum Mechanical Continuum Solvation Models. *Chem. Rev.* **2005**, *105*, 2999–3094.
- (33) Lu, T. MultiWFN: A Multifunctional Wavefunction Analyzer, Version 2.1.2, <http://multiwfn.codeplex.com>.
- (34) Sing, K. S. W.; Everett, D. H.; Haul, R. A. W.; Moscou, L.; Pierotti, R. A.; Rouquerol, J.; Siemieniewska, T. Reporting Physisorption Data for Gas/Solid Systems with Special Reference to the Determination of Surface Area and Porosity. *Pure Appl. Chem.* **1985**, *57*, 603–619.
- (35) Stern, O.; Volmer, M. Über die Abklingzeit der Fluoreszenz. *Phys. Z.* **1919**, *20*, 183–188.
- (36) Lakowicz, J. R. Quenching of Fluorescence. In *Principles of Fluorescence Spectroscopy*; Springer: New York, 2006; pp 277–330.
- (37) Mayer, I. Charge, Bond Order and Valence in the AB initio SCF Theory. *Chem. Phys. Lett.* **1983**, *97*, 270–274.
- (38) Ji, S.; Yang, J.; Yang, Q.; Liu, S.; Chen, M.; Zhao, J. Tuning the Intramolecular Charge Transfer of Alkynylpyrenes: Effect on Photophysical Properties and Its Application in Design of OFF–ON Fluorescent Thiol Probes. *J. Org. Chem.* **2009**, *74*, 4855–4865.
- (39) Li, X.-N.; Wu, Z.-J.; Liu, X.-J.; Zhang, H.-J. Origin of Rare and Highly Efficient Phosphorescent and Electroluminescent Iridium(III) Complexes Based on C≡N Ligands, A Theoretical Explanation. *J. Phys. Chem. A* **2010**, *114*, 9300–9308.